

High Fidelity Quantum Gates for Trapped Ions under Micromotion

C. Shen and L.-M. Duan

*Department of physics, University of Michigan, Ann Arbor, MI 48109 and
Center for Quantum Information, IIIS, Tsinghua University, Beijing 100084, China*

Two or three dimensional Paul traps can confine a large number of ions forming a Wigner crystal, which would provide an ideal architecture for scalable quantum computation except for the micromotion, an issue that is widely believed to be the killer for high fidelity quantum gates. Surprisingly, here we show that the micromotion is not an obstacle at all for design of high fidelity quantum gates, even though the magnitude of the micromotion is significantly beyond the requirement of the Lamb-Dicke condition. Through exact solution of the quantum Mathieu equations, we demonstrate the principle of the gate design under micromotion using two ions in a quadrupole Paul trap as an example. The proposed micromotion quantum gates can be extended to the many ion case, paving a new way for scalable trapped ion quantum computation.

PACS numbers: 03.67.Lx, 03.67.Ac, 37.10.Ty

Trapped ions constitute one of the most promising systems for realization of quantum computation [1]. All the quantum information processing experiments so far are done in linear Paul traps, where the ions form a one-dimensional (1D) crystal along the trap axis [1–4]. In this configuration, the external radio-frequency (r.f.) Paul trap can be well approximated by a static trapping potential with negligible micromotion, which is believed to be critical for design of high fidelity quantum gates. However, in term of scalability, the linear configuration is not the optimal one for realization of large scale quantum computation: first, the number of ions in a linear trap is limited [5]; and second, the linear configuration is not convenient for realization of fault-tolerant quantum computation. The effective qubit coupling in a large ion chain is dominated by the dipole interaction, which is only good for short-range quantum gates because of its fast decay with distance. In a linear chain with short range quantum gates, the error threshold for fault tolerance is very tough and hard to be met experimentally [6, 7].

From a scalability point of view, two (2D) or three dimensional (3D) Paul traps would be much better for quantum computation compared with a linear chain. In a 2D or 3D trap, one can hold a large number of qubits with a high error threshold for fault tolerance, in the range of a percent level, even with just the nearest neighbor quantum gates [7]. Thousands to millions of ions have been successfully trapped to form 2D or 3D Wigner crystals in a Paul trap [8]. However, there is a critical problem to use this system for quantum computation, i.e., the micromotion issue. In the 2D or 3D configuration, micromotion cannot be compensated, and the magnitude of micromotion for each ion can be significantly beyond the optical wavelength (i.e., outside of the Lamb-Dicke region). As the micromotion is from the driving force of the Paul trap, it cannot be laser cooled. The messy and large-magnitude micromotion well beyond the Lamb-Dicke condition is believed to be a critical hurdle for design of entangling quantum gate operations in this archi-

ture.

In this paper, we show that the micromotion surprisingly is not an obstacle at all for design of high-fidelity quantum gates. When the ions form a crystal in a time-dependent Paul trap, they will be described by a set of Mathieu equations. We solve exactly the quantum Mathieu equations in general with an inhomogeneous driving term and find that the micromotion is dominated by a well-defined classical trajectory with no quantum fluctuation. This large classical motion is far outside of the Lamb-Dicke region, however, it does not lead to infidelity of quantum gates if it is appropriately taken into account in the gate design. The quantum part of the Mathieu equation is described by the secular mode with a micromotion correction to its mode function. This part of motion still satisfies the Lamb-Dicke condition at the Doppler temperature, which is routine to achieve for experiments. We use two ions in a quadrupole trap, which have large micromotion, as an example to show the principle of the gate design, and give the explicit gate scheme both in the slow and the fast gate regions using multi-segment laser pulses [9, 10], with the intrinsic gate infidelity arbitrarily approaching zero under large micromotion. We finally give a brief discussion of the general procedure of the gate design under micromotion, which in principle can work for any number of ions, with important implication for large-scale quantum computation.

To illustrate the general feature of micromotion in a Paul trap and the principle of the gate design under micromotion, we consider a three-dimensional (3D) anisotropic quadrupole trap with a time dependent potential $\Phi(x, y, z) = (U_0 + V_0 \cos(\Omega_T t)) \left(\frac{x^2 + y^2 - 2z^2}{d_0^2} \right) \equiv \alpha(t)(x^2 + y^2 - 2z^2)$ from an electric field oscillating at the r.f. Ω_T , where U_0, V_0 are voltages for the d.c. and a.c. components and d_0 characterizes the size of the trap. We choose a positive U_0 to reduce the effective trap strength along the z direction so that the two ions align along the z -axis. Since the motions in different directions do not

couple to each other under quadratic expansion, we focus our attention on the z direction. The total potential energy of two ions (each with charge e and mass m) is

$$V(z_1, z_2) = -2e\alpha(t) (z_1^2 + z_2^2) + \frac{e^2}{4\pi\epsilon_0 |z_1 - z_2|}. \quad (1)$$

Define center-of-mass (CM) coordinate $u_{\text{cm}} = (z_1 + z_2)/2$ and relative coordinate $u_r = z_1 - z_2$. Without loss of generality, we assume $u_r > 0$ and its average $\bar{u}_r = u_0$. We assume the magnitude of the ion motion is significantly less than the ion separation, which is always true for the ions in a crystal phase. The Coulomb interaction can then be expanded around the average distance \bar{u}_r up to the second order of $|u_r - u_0|$. Under this expansion, the total Hamiltonian $H = p_{\text{cm}}^2/4m + p_r^2/m + V(z_1, z_2)$ is quadratic (although time-dependent) in terms of the coordinate operators u_{cm}, u_r and the corresponding momentum operators $p_{\text{cm}} = p_1 + p_2, p_r = (p_1 - p_2)/2$. The Heisenberg equations under this Hamiltonian H yield the following quantum Mathieu equations respectively for the coordinate operators u_{cm} and u_r

$$\frac{d^2 u_{\text{cm}}}{d\xi^2} + (a_{\text{cm}} - 2q_{\text{cm}} \cos(2\xi)) u_{\text{cm}} = 0 \quad (2)$$

$$\frac{d^2 u_r}{d\xi^2} + (a_r - 2q_r \cos(2\xi)) u_r = f_0 \quad (3)$$

where the dimensionless parameters $a_{\text{cm}} = -16eU_0/(md_0^2\Omega_T^2)$, $a_r = a_{\text{cm}} + 4e^2/(\pi\epsilon_0 mu_0^3\Omega_T^2)$, $q_{\text{cm}} = q_r = 8eV_0/(md_0^2\Omega_T^2)$ and the dimensionless time $\xi = \Omega_T t/2$. The driving term $f_0 = 6e^2/(\pi\epsilon_0 mu_0^3\Omega_T^2)$. The quantum operators u_{cm} and u_r satisfy the same form of the Mathieu equations (except for the driving term f_0) as for the classical variables. As these equations are linear, we can use the solutions known for the classical Mathieu equation to construct a quantum solution that takes into account of the quantum fluctuation.

It is well known that the solution to the classical Mathieu equation $\frac{d^2 v}{d\xi^2} + (a - 2q \cos(2\xi)) v = 0$ is a combination of Mathieu sine $S(a, q, \xi)$ and Mathieu cosine $C(a, q, \xi)$ functions, which reduce to the conventional sine and cosine functions when micromotion is neglected [11]. The solution to a homogeneous quantum Mathieu equation $\frac{d^2 \hat{u}}{d\xi^2} + (a - 2q \cos(2\xi)) \hat{u} = 0$ can be described using the reference oscillator technique [12]. From the classical solution v and the quantum operator \hat{u} , one can introduce the following annihilation operator of a reference oscillator (remember that $\xi = \Omega_T t/2$ is the dimensionless time)

$$\hat{a}(t) = \sqrt{\frac{m}{2\hbar\omega}} i \left(v(t) \dot{\hat{u}}(t) - \dot{v}(t) \hat{u}(t) \right), \quad (4)$$

where ω is a normalization constant typically taken as the secular motion frequency of the corresponding Mathieu equation. In addition, we impose the initial condition for $v(t)$ with $v(t)|_{t=0} = 1$ and $\dot{v}(t)|_{t=0} = i\omega$.

The position operator $\hat{u}(t)$ and its conjugate momentum $\hat{p}(t) \equiv m\dot{\hat{u}}(t)$ satisfy the commutator $[\hat{u}(t), \hat{p}(t)] = i\hbar$. From the above definition, one can easily check that $\frac{d}{dt}\hat{a}(t) \propto v\frac{d^2}{d\xi^2}\hat{u} - \hat{u}\frac{d^2}{d\xi^2}v = 0$, so $\hat{a}(t) \equiv \hat{a}$ is a constant of motion. Furthermore, \hat{a} and \hat{a}^\dagger satisfy the standard commutator

$$[\hat{a}, \hat{a}^\dagger] = (m/2\hbar\omega) (i\hbar/m) (v(t)\dot{v}^*(t) - v^*(t)\dot{v}(t))|_{t=0} = 1.$$

When micromotion is neglected, $v(t) = e^{i\omega t}$ and \hat{a} reduces to the annihilation operator of a harmonic oscillator. In the presence of micromotion, $v(t) = C(a, q, \xi) + iS(a, q, \xi)$. The solution to the position operator \hat{u} takes the form

$$\hat{u}(t) = u_0 (v^*(t)\hat{a} + v(t)\hat{a}^\dagger) \quad (5)$$

where $u_0 \equiv \sqrt{\hbar/2m\omega}$ is the oscillator length.

The above solution gives a complete description of the center-of-mass motion with the operator

$$u_{\text{cm}}(t) = u_{0\text{cm}} (v_{\text{cm}}^*(t)\hat{a}_{\text{cm}} + v_{\text{cm}}(t)\hat{a}_{\text{cm}}^\dagger), \quad (6)$$

where $u_{0\text{cm}} \equiv \sqrt{\hbar/4m\omega_{\text{cm}}}$ and ω_{cm} is the secular frequency of the center of mass mode. The relative motion u_r satisfies the inhomogeneous quantum Mathieu equation (3). To solve it, we let $u_r = u_r' + \bar{u}_r$, where u_r' is an operator that inherits the commutators for u_r and satisfies the homogenous quantum Mathieu equation and \bar{u}_r is a classical variable corresponding to a special solution of the Mathieu equation $\frac{d^2 \bar{u}_r}{d\xi^2} + (a_r - 2q_r \cos(2\xi)) \bar{u}_r = f_0$. The special solution \bar{u}_r can be found through the series expansion $\bar{u}_r = f_0 \sum_{n=0}^{+\infty} c_n \cos(2n\xi)$, where the expansion coefficients c_n satisfy the recursion relations $a_r c_0 - q_r c_1 = 1$ and $c_n = D_n (c_{n-1} + c_{n+1} + c_0 \delta_{n,1})$ for $n \geq 1$ with $D_n \equiv -q_r/(4n^2 - a_r)$. When $a_r \ll 1$ and $q_r \ll 1$, which is typically true under real experimental configurations, c_n rapidly decays to zero with $|c_{n+1}/c_n| \approx q_r/4(n+1)^2$ and we can keep only the first few terms in the expansion and obtain an approximate analytical expression for \bar{u}_r [13]. The complete solution of u_r is then given by

$$u_r(t) = u_{0r} (v_r^*(t)\hat{a}_r + v_r(t)\hat{a}_r^\dagger) + \bar{u}_r(t), \quad (7)$$

where $u_{0r} \equiv \sqrt{\hbar/m\omega_r}$ and ω_r is the secular frequency of the relative mode.

Now we show how to design high fidelity quantum gates under micromotion. To perform the controlled phase flip (CPF) gate, we apply laser induced spin dependent force on the ions, with the interaction Hamiltonian described by [10]

$$H = \sum_{j=1}^2 \hbar \Omega_j \cos(k_\delta z_j + \mu_\delta t + \phi_j) \sigma_j^z. \quad (8)$$

where k_δ is the wave vector difference of the two Raman beams along the z direction, μ_δ is the two-photon Raman detuning, Ω_j (real) is the Raman Rabi frequency

for the ion j , and ϕ_j is the corresponding initial phase. In terms of the normal modes, the position operators $z_j = u_{\text{cm}} - (-1)^j u_{\text{r}}/2$, where $u_{\text{cm}}, u_{\text{r}}$ are given by Eqs. (6) and (7). We introduce three Lamb-Dicke parameters, $\eta_{\text{cm}} \equiv k_\delta u_{0\text{cm}}$ for the CM mode, $\eta_{\text{r}} \equiv k_\delta u_{0\text{r}}/2$ for the relative mode, and $\eta_{\text{mm}} \equiv k_\delta \bar{u}_{\text{r}}/2$ for pure micromotion. Under typical experimental configurations, $\eta_{\text{cm}} \sim \eta_{\text{r}} \ll 1$. The parameter η_{mm} is a classical variable that oscillates rapidly with time by multiples of the micromotion frequency Ω_T . In Fig. 1(a), we show a typical trajectory of $\eta_{\text{mm}}(t)$. The magnitude of variation of η_{mm} is considerably larger than 1. In Fig. 1(b), we also plot the function $v_{\text{cm}}(t)$, which is dominated by the oscillation at the secular motion frequency ω_{cm} with small correction from the micromotion. The magnitude of $v_{\text{cm}}(t)$ is bounded by a constant slightly larger than 1. The function $v_{\text{r}}(t)$ has very similar behavior except that ω_{cm} is replaced by ω_{r} . From this consideration of parameters, we can expand the term $\cos(k_\delta z_j + \mu_\delta t + \phi_j)$ with small parameters $\eta_{\text{cm}}, \eta_{\text{r}}$, but η_{mm} is a big term which needs to be treated exactly. After the expansion, to leading order in η_{cm} and η_{r} , the Hamiltonian H takes the form

$$H \approx -[\chi_1(t)\sigma_1^z + \chi_2(t)\sigma_2^z]\hat{f}_{\text{cm}} - [\chi_1(t)\sigma_1^z - \chi_2(t)\sigma_2^z]\hat{f}_{\text{r}}, \quad (9)$$

where we have defined

$$\hat{f}_\mu \equiv \eta_\mu \left(v_\mu^*(t)\hat{a}_\mu + v_\mu(t)\hat{a}_\mu^\dagger \right), \quad (10)$$

$$\chi_j(t) \equiv \hbar\Omega_j \sin[\mu_\delta t + \phi_j - (-1)^j \eta_{\text{mm}}(t)], \quad (11)$$

where the subscript $\mu = \text{cm}, \text{r}$ and $j = 1, 2$. In Eq. (9), we have dropped the term $\cos(\mu_\delta t + \phi_j \pm \eta_{\text{mm}})$ which induces single-bit phase shift but is irrelevant for the CPF gate. The evolution operator at the gate time τ generated by the Hamiltonian H can be expressed as

$$U(\tau) = D_{\text{cm}}(\alpha_{\text{cm}})D_{\text{r}}(\alpha_{\text{r}})\exp[i(\gamma_{\text{r}} - \gamma_{\text{cm}})\sigma_1^z\sigma_2^z], \quad (12)$$

where the displacement operator $D_\mu(\alpha_\mu) \equiv \exp(\alpha_\mu\hat{a}_\mu^\dagger - \alpha_\mu^*\hat{a}_\mu)$ ($\mu = \text{cm}, \text{r}$). Let $j_\mu = 1$ for $\mu = \text{cm}$ and $j_\mu = -1$ for $\mu = \text{r}$. The displacement α_μ and the accumulated phase γ_μ have the following expression

$$\alpha_\mu = i\eta_\mu \int_0^\tau (\chi_1(t)\sigma_1^z + j_\mu\chi_2(t)\sigma_2^z) u_\mu(t) dt \quad (13)$$

$$\gamma_\mu = i(\eta_\mu)^2 \int_0^\tau dt_1 \int_0^{t_1} dt_2 \mathcal{S}[\chi_1\chi_2] \text{Im}[u_\mu(t_1)u_\mu^*(t_2)] \quad (14)$$

where $\mathcal{S}[\chi_1\chi_2] \equiv \chi_1(t_1)\chi_2(t_2) + \chi_1(t_2)\chi_2(t_1)$.

To realize the CPF gate, we require $\alpha_\mu = 0$ and $\gamma_{\text{r}} - \gamma_{\text{cm}} = \pi/4$. The integrals α_μ can be evaluated semi-analytically [13] or purely numerically. We normally take $\Omega_1 = \Omega_2 \equiv \Omega$. Note that even in this case $\chi_1(t_1) \neq \chi_2(t_2)$ with the micromotion term $\eta_{\text{mm}}(t)$. This is different from the case of a static trap. From Eq. (12), we see that

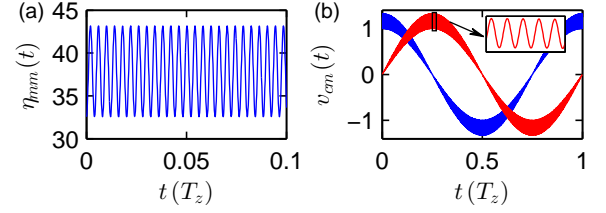


Figure 1: (Color online) (a) The time dependent parameter $\eta_{\text{mm}}(t)$ and (b) the function $v_{\text{cm}}(t)$. The real/imaginary part (blue/red curves) of $v_{\text{cm}}(t)$ has even/odd parity as a function of time and looks similar to \cos/\sin function. Unit of time is the trap frequency $T_z = 2\pi/\omega_{\text{cm}}$. The parameters used are: ion mass $m = 9u$ (u is the atomic mass unit) corresponding to Be^+ ; r.f. trap frequency $\Omega_T = 2\pi \times 240\text{MHz}$; the characteristic electrode size $d_0 = 200\text{ }\mu\text{m}$; AC/DC voltages V_0, U_0 are 300V and 21V respectively. The resulting secular trap frequencies are $\omega_{\text{cm}} = 2\pi \times 0.965\text{MHz}$, $\omega_{\text{r}} = 2\pi \times 3.62\text{MHz}$ along the z -axis, and $\omega_x = \omega_y = 2\pi \times 20.8\text{MHz}$ along x - and y -axis.

$\alpha_\mu = 0$ for a fixed μ gives two complex and thus four real constraints. With excitation of N motional modes, the total number of (real) constraints to realize the CPF gate is therefore $4N + 1$ (the condition $\gamma_{\text{r}} - \gamma_{\text{cm}} = \pi/4$ gives one constraint). To satisfy these constraints, we divide the Rabi frequency $\Omega(t)$ ($0 \leq t \leq \tau$) into m equal-time segments, and take a constant Ω_β ($\beta = 1, 2, \dots, m$) for the β th segment [9, 10]. This kind of modulation can be conveniently done through an acoustic optical modulator in experiments [14]. The Rabi frequencies are our control parameters. For the two ion case, under fixed detuning μ_δ and gate time τ , in general we can find a solution for the CPF gate with $m = 9$ segments. For some specific detuning μ_δ very close to a secular mode frequency, off-resonant excitations become negligible and a solution is possible under one segment of pulse by tuning of the gate time τ , which corresponds to the case of the Sørensen-Mølmer gate [3] generalized to include the micromotion correction.

To characterize the quality of the gate, we use the fidelity $F \equiv \text{tr}_\mu \left[\rho_\mu \left| \langle \Psi_0 | U_{\text{CPF}}^\dagger U(\tau) | \Psi_0 \rangle \right|^2 \right]$, defined as the overlap of the evolution operator $U(\tau)$ with the perfect one $U_{\text{CPF}} \equiv e^{i\pi\sigma_1^z\sigma_2^z/4}$ under the initial state $|\Psi_0\rangle$ for the ion spins and the thermal state ρ_μ for the phonon modes. In our calculation, without loss of generality, we take $|\Psi_0\rangle = (|0\rangle + |1\rangle) \otimes (|0\rangle + |1\rangle)/2$ and assume the Doppler temperature T_D for all the phonon modes. For any given detuning μ_δ and gate time τ , we optimize the control parameters Ω_β ($\beta = 1, 2, \dots, m$) to get the maximum fidelity F . In Fig. (2), we show the gate fidelity as a function of gate time for $\mu_\delta = 0.95\omega_{\text{cm}}$ (close to a secular frequency) by applying a single segment laser pulse of a constant Rabi frequency Ω . In the figure, the dashed line corresponds to the result in a static harmonic trap

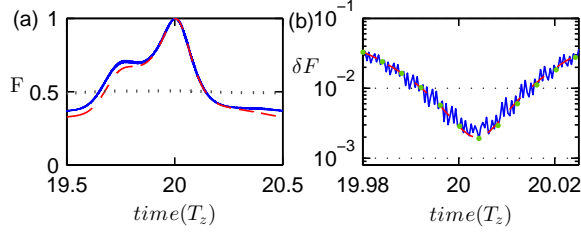


Figure 2: (Color online) (a) The fidelity of a two-ion conditional phase flip gate as a function of gate time, with the unit of time $T_z = 2\pi/\omega_{cm}$. The detuning was chosen to be $\mu = 0.95\omega_{cm}$. Blue solid line indicates the optimal results with micromotion taken into account; red dashed line is the result for a genuine static harmonic trap without micromotion; gray dotted line is obtained by applying the optimal solution for a static harmonic trap to the case with micromotion, which results in poor performance. (b) The infidelity ($\delta F \equiv 1 - F$) near the optimal evolution time, essentially a zoom-in of panel (a) near $t = 20T_z$. Green dots in (b) show the time points that are an integral multiple of the micromotion period. Other parameters used are: Doppler temperature for both motional degrees of freedom with $k_B T_D \approx 10\hbar\omega_{cm}$; effective laser wave vector $\Delta k = 8\mu\text{m}^{-1}$ so $\eta_{cm} \approx 0.12$ and $\eta_r \approx 0.09$.

with the same secular frequencies but no micromotion. If we take into account the micromotion contribution but do not change the gate design, the result is described by the dash-dot line, with a low fidelity about only 50%. When we optimize the gate design (optimize Ω_β) including the micromotion correction, the gate fidelity is represented by the solid line, which approaches the optimal fidelity achievable in a static trap. The gate infidelity $\delta F \equiv 1 - F$ approaches 2×10^{-3} at the optimal gate time $\tau = 20.005T_z$, where $T_z \equiv 2\pi/\omega_{cm}$.

By applying 9 segments of laser pulses with optimized Ω_β ($\beta = 1, 2, \dots, 9$), the gate fidelity F can attain the unity at arbitrary detuning μ_δ for the two ion case. As an example, In Fig. 3(a), we show the optimized solution of Ω_β (blue lines) at an arbitrarily chosen detuning $\mu_\delta = 1.4\omega_{cm}$. For comparison, the red lines represent the solution of Ω_β in a static harmonic trap with otherwise the same parameters. The maximum magnitude of $|\Omega_\beta|$ significantly increases in the presence of micromotion. This is understandable as fast oscillations of the micromotion tend to lower the effective Rabi frequencies. In Fig. 3(b), we show the maximum magnitude of $|\Omega_\beta|$ as a function of the gate time τ . Compared with the

solution in a static harmonic trap, the maximum $|\Omega_\beta|$ in general needs to increase by about an order of magnitude under micromotion.

In conclusion, we demonstrate that arbitrarily high fidelity quantum gates can be achieved under large micromotion. The demonstration in this paper uses the example of two ions in a quadrupole trap, which has the micromotion magnitude significantly beyond the Lamb-

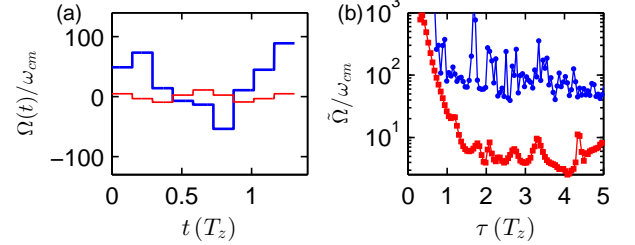


Figure 3: (Color online) (a) The waveform of the optimal segmented pulse calculated for the gate with duration $\tau = 1.31T_z$. The thick blue (thin red) line corresponds to the case with (without) micromotion. (b) The maximal Rabi frequency $\tilde{\Omega} \equiv \max_t |\Omega(t)|$ as a function of the gate time τ . The upper blue (lower red) curve corresponds to the case with (without) micromotion.

Dicke limit. Apparently, the idea here is applicable to the many ion case. For a system of N ions in any dimension, as long as the ions crystallize, each ion has an average equilibrium position. We can then expand the Coulomb potential around these equilibrium positions. Under the r.f. Paul trap and the Coulomb interaction, the motion of the ions can then be described by a set of coupled time-dependent Mathieu equations. Using the technique in this paper, we can solve the motional dynamics and optimize the gate design that explicitly takes into account all the micromotion contributions. The gate design technique under micromotion proposed in this paper solves a major obstacle for high fidelity quantum computation in real r.f. traps beyond the 1D limitation and opens a new way for scalable quantum computation based on large 2D or 3D trap-ion crystals in Paul traps.

Acknowledgments. This work was supported by the NBRPC (973 Program) 2011CBA00300 (2011CBA00302), the IARPA MUSIQ program, the ARO and the AFOSR MURI programs, and the DARPA OLE program.

Appendix: Supplementary Material

In this appendix, we show in detail how to solve the driven Mathieu equation and give an approximate treatment of the motional integrals.

SOLUTION OF DRIVEN MATHIEU EQUATION

We show in detail how to solve the Mathieu equation with a constant drive term.

$$\frac{d^2 u}{d\xi^2} + (a - 2q \cos(2\xi)) u = f_0$$

Let us assume that $u(\xi) = f_0 \sum_{n=0}^{\infty} c_n \cos(2n\xi)$ and insert it into the equation. After re-organization, we get

$$ac_0 - qc_1 + \sum_{n=1}^{\infty} [(a - 4n^2)c_n - q(c_{n-1} + c_{n+1}) - qc_0\delta_{n,1}] \cos(2nt) = 1.$$

Defining $D_n \equiv (a - 4n^2)/q$, we have the following set of linear equations

$$\begin{aligned} ac_0 - qc_1 &= 1 \\ c_n - \frac{1}{D_n}(c_{n-1} + c_{n+1} + c_0\delta_{n,1}) &= 0. \end{aligned}$$

In matrix form,

$$\begin{pmatrix} a & -q & 0 & \cdots & 0 \\ -\frac{2}{D_1} & 1 & -\frac{1}{D_1} & & \\ 0 & -\frac{1}{D_2} & 1 & -\frac{1}{D_2} & \\ \vdots & & -\frac{1}{D_3} & 1 & -\frac{1}{D_3} \\ & & & \ddots & \ddots \\ 0 & & & & \end{pmatrix} \cdot \begin{pmatrix} c_0 \\ c_1 \\ c_2 \\ \vdots \end{pmatrix} = \begin{pmatrix} 1 \\ 0 \\ 0 \\ \vdots \end{pmatrix}. \quad (15)$$

The factor $1/D_n$ decreases very fast as n increases and we can truncate the expansion of $u(\xi)$ at a small n . Numerically we observe that typically keeping up to c_2 already gives enough accuracy. We can thus get a very accurate analytical expression

$$\begin{aligned} c_0 &\approx \frac{64 + a(a - 20) - q^2}{(32 - 3a)q^2 + a(a - 4)(a - 16)}, \\ c_1 &\approx \frac{2(a - 16)q}{(32 - 3a)q^2 + a(a - 4)(a - 16)}, \\ c_2 &\approx \frac{2q^2}{(32 - 3a)q^2 + a(a - 4)(a - 16)}. \end{aligned}$$

For the example in the main text, $a_r = -0.0388$ and $q_r = 0.283$, we have $c_0 = 1132.8$ and $u_r(\xi) = f_0 c_0 [1 - 0.14 \cos(2\xi) + 0.0025 \cos(4\xi) + \cdots]$.

The micromotion corrected equilibrium position is $f_0 c_0$ and should be identified with u_0 around which we expand the Coulomb potential in the first place. Thus we should determine them self-consistently. Taking the relative motion in the manuscript as an example, since both $a_r \equiv \frac{-16eU_0}{md_0^2\Omega_T^2} + \frac{4e^2}{\pi\epsilon_0 m u_0^3 \Omega_T^2}$ and $f_0 \equiv \frac{6e^2}{\pi\epsilon_0 m u_0^2 \Omega_T^2}$ are functions of u_0 , then the self-consistent equation

$$u_0 = f_0 c_0 \approx f_0 \frac{64 + a_r(a_r - 20) - q_r^2}{(32 - 3a_r)q_r^2 + a_r(a_r - 4)(a_r - 16)}$$

gives the correct u_0 . With the iterative method it typically takes only a few iterations to converge to the correct value when starting from a proper initial value of u_0 .

TWO-STAGE TIME INTEGRAL

Here we offer an approximate treatment of motional integrals. We notice that the secular frequency ω and the micromotion frequency Ω are well separated, i.e. $\omega \ll \Omega$. This means quantities with characteristic frequency ω or

below stay constant within one period of micromotion. So we can perform the time integral in two steps: we first integrate over one period of the micromotion, obtaining a slowly varying integrand, which we then integrate again. By doing this we will show that the dominant effect of micromotion is to modulate the effective Rabi frequency. Notice that the integrals $\int_0^\tau \chi(t)u(t) dt$ can be reduced to the form below (ignoring micromotion frequencies $n\Omega \pm \omega$ with $n \geq 2$)

$$I = \int_0^\tau \sin(a_0(t) + a_1(t) \cos(\Omega t_1 + \phi(t))) (b_0(t) + b_1(t) \cos(\Omega t + \varphi(t)))$$

where $a_0(t)$, $a_1(t)$, $b_0(t)$, $b_1(t)$, $\phi(t)$ and $\varphi(t)$ are all real slowly varying functions within one period of micromotion $\frac{2\pi}{\Omega}$. The above integral can be further broken into two parts, I_1 and I_2 , where

$$\begin{aligned} I_1 &\approx \int_0^\tau dt \frac{\Omega}{2\pi} \int_t^{t+2\pi/\Omega} dt_1 \sin(a_0(t) + a_1(t) \cos(\Omega t_1 + \phi)) b_0(t) \\ &= \int_0^\tau dt \frac{1}{2\pi} \int_{-\pi}^\pi dt' \sin(a_0(t) + a_1(t) \cos(t')) b_0(t) \\ &= \text{Im} \left[\int_0^\tau dt \exp(i a_0(t)) \frac{1}{2\pi} \int_{-\pi}^\pi dt' \exp(i a_1 \cos(t')) b_0(t) \right] \\ &\quad \text{Im} \left[\int_0^\tau dt \exp(i a_0(t)) J_0(a_1) b_0(t) \right] \\ &= \int_0^\tau dt \sin(a_0(t)) b_0(t) J_0(a_1(t)) \end{aligned}$$

and

$$\begin{aligned} I_2 &= \int_0^\tau dt \sin(a_0(t) + a_1(t) \cos(\Omega t + \phi)) b_1(t) \cos(\Omega t + \varphi(t)) \\ &\approx \int_0^\tau dt \frac{\Omega}{2\pi} \int_t^{t+2\pi/\Omega} dt_1 \sin(a_0(t) + a_1(t) \cos(\Omega t_1 + \phi)) b_1(t) \cos(\Omega t_1 + \varphi) \\ &= \int_0^\tau dt \cos(a_0(t)) \cos(\varphi - \phi) J_1(a_1(t)) \end{aligned}$$

where J_0 and J_1 denote the Bessel functions. In both cases, the micromotion gives rise to slowly varying modulation factors, $J_0(a_1(t))$ and $\cos(\varphi - \phi) J_1(a_1(t))$. Moreover in I_2 the phase of the original integrand is also shifted, $\sin(a_0(t)) \rightarrow \cos(a_0(t))$. For the actual experimental system, the term I_2 contributes much less than the I_1 to the target integral I , due to the much smaller coefficient of the micromotion component than that of the secular component in $v(t)$. So in leading order, micromotion reduces the laser Rabi frequency seen by the ion by a factor on the order of $J_0(a_1(t))$.

-
- [1] For a review, see D. Leibfried, R. Blatt, C. Monroe, D. Wineland, Rev. Mod. Phys. 75, 281-324 (2003); R. Blatt and D. Wineland, Nature 453, 1008-1015 (2008); C. Monroe, J. Kim, Science 339, 1164-1169 (2013).
[2] J. I. Cirac and P. Zoller, Phys. Rev. Lett. 74, 4091-4094 (1995).
[3] A. Sørensen and K. Mølmer, Phys. Rev. Lett. 82, 1971 (1999); G. J. Milburn, S. Schneider, and D. F. V. James, Fortschr. Physik 48, 801-810 (2000); A. Sørensen, K. Mølmer, Phys. Rev. A 62, 022311 (2000).
[4] C. A. Sackett, et. al., Nature 404, 256 (2000); D. Leibfried et al., Nature 422, 412-415 (2003); F. Schmidt-Kaler, et. al., Nature 422, 408 (2003); H. Häffner, et.al, Nature, 438, 643 (2005); J. Benhelm, G. Kirchmair, C. F. Roos, and R. Blatt, Nature Physics 4, 463 (2008); K. Kim,

- et. al., Nature 465, 590 (2010); R. Islam, et al., Nature Comm. 2, 377 (2011); B. P. Lanyon, et. al., Science 334, 57 (2011); B. P. Lanyon, et. al., Phys. Rev. Lett. 111, 210501 (2013); R. Islam, et. al., Science 340, 583 (2013).
[5] M. G. Raizen, J. M. Gilligan, J. C. Bergquist, W. M. Itano, and D. J. Wineland, Phys. Rev. A 45, 6493 (1992); J. P. Schiffer, Phys. Rev. Lett. 70, 818 (1993); G.-D. Lin, et al., Europhys. Lett. 86, 60004 (2009).
[6] D. Gottesman, J. Mod. Opt. 47, 333-345 (2000); T. Szkopek et al., IEEE Trans. Nano., Vol. 5, No. 1, pp 42-49, 2006.
[7] R. Raussendorf and J. Harrington, Phys. Rev. Lett. 98, 190504 (2007).
[8] A. Mortensen, E. Nielsen, T. Matthey, and M. Drewsen, Phys. Rev. Lett. 96, 103001 (2006); K. Okada, T. Takayanagi, M. Wada, S. Ohtani, and H. A. Schuessler, Phys. Rev. A 80, 043405 (2009); B. Szymanski, et. al., App. Phys. Lett. 100, 171110 (2012); M.

- Drewsen, T. Matthey, A. Mortensen, and J. P. Hansen, arXiv:1202.2544 (2012).
- [9] S.-L. Zhu, C. Monroe, and L.-M. Duan, *Europhys. Lett.* 73, 485 (2006).
 - [10] S.-L. Zhu, C. Monroe, and L.-M. Duan, *Phys. Rev. Lett.* 97, 050505 (2006).
 - [11] N. W. McLachlan, *Theory and Application of Mathieu Functions* (Clarendon Press, Oxford, 1947).
 - [12] M. Combescure, *Annales de l'institut Henri Poincare (A) Physique theorique* 44, 293 (1986); L. S. Brown, *Phys. Rev. Lett.* 66, 527 (1991); R. J. Glauber, in *Laser Manipulation of Atoms and Ions* (1922), vol. 118 of *Proceedings of the International School of Physics "Enrico Fermi" Course*; B. E. King, Ph.D. thesis, University of Colorado at Boulder (1999).
 - [13] See supplementary material in the appendix for details of the solution of the inhomogeneous Mathieu equation and an approximate treatment of the motional integrals.
 - [14] T. Choi, S. Debnath, T. A. Manning, C. Figgatt, Z.-X. Gong, L.-M. Duan, and C. Monroe, arXiv:1401.1575 (2014).